Measuring Chromatin Interaction Dynamics on the Second Time Scale at Single-Copy Genes

Kunal Poorey *et al.*

Science **342**, 369 (2013);
DOI: 10.1126/science.1242369

Some inhibitory factors produced by other fungi are cell-wall components (*23*); therefore, factors produced by *B. dendrobatidis* may also be located in the cell wall. This idea is consistent with the failure of zoospores, which lack a cell wall, to inhibit. To determine whether inhibitory factors are derived from the cell wall, we interfered with cell-wall synthesis using nikkomycin Z (NZ), a chitin synthase inhibitor (*24*). Preculturing *B. dendrobatidis* with NZ significantly decreased inhibition by both *B. dendrobatidis* cells and supernatants (Figs. 4, C and D). These experiments, along with the observation that noninhibitory zoospores lack cell walls, suggest that the inhibitory factors produced by *B. dendrobatidis* are cell-wall components. Chitin and β-1,3-glucan are the main structural cell-wall components of many fungi (*25*). Therefore, we conducted experiments to determine whether they might be inhibitory. Treatment of *B. dendrobatidis* supernatants with β-glucanases and chitinases did not affect the inhibitory activity (fig. S16). Furthermore, treatment of proliferating lymphocytes with a soluble β-glucan (laminarin) did not inhibit function (fig. S16). Thus, the inhibitory factor does not appear to be a β-glucan or chitin.

We conclude that *B. dendrobatidis*, like other pathogenic fungi, produces toxic factors that inhibit potentially protective host immune responses and likely impair the function of other cells in close proximity. Soluble molecules released by *B. dendrobatidis* inhibited proliferation of amphibian and mammalian lymphocytes and induced apoptosis of target cells by activating both intrinsic and extrinsic pathways. The role of phagocytic cells (macrophages and neutrophils) in controlling chytridiomycosis is not yet well understood. These cells can engulf *B. dendrobatidis*, and accessory functions do not appear to be impaired by *B. dendrobatidis* supernatants. Because these soluble mycotoxins inhibited proliferation and caused death of nonlymphoid cell lines, they are more broadly cytotoxic and could be responsible for other symptoms of chytridiomycosis including disruption of the skin (*2*, *7*, *26*) and behavioral changes, such as lethargy and loss of righting reflex (*6*, *7*). One or more of the factors produced by *B. dendrobatidis* may be derived from the cell wall. The capacity of *B. dendrobatidis* to evade protective immune responses helps to explain how this fungus can be so lethal to amphibians lacking effective innate defenses (*27*) and why some amphibian species with more robust innate responses persist with mild infections as *B. dendrobatidis* reservoirs (*28*–*30*).

References and Notes

1. J. P. Collins, *Dis. Aquat. Organ.* **92**, 93–99 (2010).
2. L. Berger *et al.*, *Proc. Natl. Acad. Sci. U.S.A.* **95**, 9031–9036 (1998).
3. J. E. Longcore, A. P. Pessier, D. K. Nichols, *Mycologia* **91**, 219 (1999).
4. L. F. Skerratt *et al.*, *EcoHealth* **4**, 125–134 (2007).
5. J. P. Ramsey, L. K. Reinert, L. K. Harper, D. C. Woodhams, L. A. Rollins-Smith, *Infect. Immun.* **78**, 3981–3992 (2010).
6. A. P. Pessier, D. K. Nichols, J. E. Longcore, M. S. Fuller, *J. Vet. Diagn. Invest.* **11**, 194–199 (1999).
7. J. Voyles, E. B. Rosenblum, L. Berger, *Microbes Infect.* **13**, 25–32 (2011).
8. E. B. Rosenblum *et al.*, *PLoS ONE* **4**, e6494 (2009).
9. L. Ribas *et al.*, *PLoS ONE* **4**, e8408 (2009).
10. J. R. Collette, M. C. Lorenz, *Curr. Opin. Microbiol.* **14**, 668–675 (2011).
11. G. D. Brown, *Annu. Rev. Immunol.* **29**, 1–21 (2011).
12. L. A. Rollins-Smith, S. C. V. Parsons, N. Cohen, *Immunology* **52**, 491–500 (1984).
13. H. Morales, A. Muharemagic, J. Gantress, N. Cohen, J. Robert, *Cell Stress Chaperones* **8**, 265–271 (2003).
14. Detailed materials and methods are available as supplementary materials on *Science* Online.
15. S. Joneson, J. E. Stajich, S.-H. Shiu, E. B. Rosenblum, *PLoS Pathog.* **7**, e1002338 (2011).
16. A. Vecchiarelli, C. Monari, *Mycopathologia* **173**, 375–386 (2012).
17. R. Ben-Ami, R. E. Lewis, D. P. Kontoyiannis, *Br. J. Haematol.* **150**, 406–417 (2010).
18. A. P. Campanelli *et al.*, *J. Infect. Dis.* **187**, 1496–1505 (2003).
19. E. Pericolini *et al.*, *J. Immunol.* **182**, 6003–6010 (2009).
20. I. Vermes, C. Haanen, H. Steffens-Nakken, C. Reutellingsperger, *J. Immunol. Methods* **184**, 39–51 (1995).
21. A. Degterev *et al.*, *Nat. Chem. Biol.* **1**, 112–119 (2005).
22. L. A. Rollins-Smith *et al.*, *Dev. Comp. Immunol.* **26**, 471–479 (2002).
23. C. A. Rappleye, L. G. Eissenberg, W. E. Goldman, *Proc. Natl. Acad. Sci. U.S.A.* **104**, 1366–1370 (2007).
24. J. P. Gaughran, M. H. Lai, D. R. Kirsch, S. J. Silverman, *J. Bacteriol.* **176**, 5857–5860 (1994).
25. F. M. Klis, P. Mol, K. Hellingwerf, S. Brul, *FEMS Microbiol. Rev.* **26**, 239–256 (2002).
26. J. Voyles *et al.*, *Science* **326**, 582–585 (2009).
27. L. A. Rollins-Smith, J. P. Ramsey, J. D. Pask, L. K. Reinert, D. C. Woodhams, *Integr. Comp. Biol.* **51**, 552–562 (2011).
28. R. Mazzoni *et al.*, *Emerg. Infect. Dis.* **9**, 995–998 (2003).
29. C. Weldon, L. H. du Preez, A. D. Hyatt, R. Muller, R. Speare, *Emerg. Infect. Dis.* **10**, 2100–2105 (2004).
30. D. C. Woodhams, A. D. Hyatt, D. G. Boyle, L. A. Rollins-Smith, *Herpetol. Rev.* **39**, 66 (2008).

Acknowledgments: This research was supported by NSF grants IOS-0619536, IOS-0843207, and IOS-1121758 (to L.A.R-S.); NIH grants AI044924 (to T.M.A.), AI007281 (to D.M.S.), AI038296 (to T.S.D.), 1K01HL103179-01, The Foundation for Sarcoidosis Research (to K.O-R.) and a dissertation enhancement grant from Vanderbilt University (to J.S.F.). W.M.H. was supported by an individual NSF Graduate Research Fellowship. We thank J. Galgiani, director of the Valley Fever Center for Excellence of the University of Arizona, for the gift of nikkomycin Z under a Materials Transfer Agreement. Anti-*Xenopus* monoclonal antibodies were provided by the University of Rochester *Xenopus laevis* Research Resource for Immunobiology. All data necessary to understand this manuscript are presented in the main text or supplementary materials.

Supplementary Materials

www.sciencemag.org/content/342/6156/366/suppl/DC1
Materials and Methods
Figs. S1 to S16
References (*31*–*66*)

16 July 2013; accepted 6 September 2013
10.1126/science.1243316

Measuring Chromatin Interaction Dynamics on the Second Time Scale at Single-Copy Genes

Kunal Poorey,[1]* Ramya Viswanathan,[1]* Melissa N. Carver,[1] Tatiana S. Karpova,[2] Shana M. Cirimotich,[1] James G. McNally,[2] Stefan Bekiranov,[1]† David T. Auble[1]†

The chromatin immunoprecipitation (ChIP) assay is widely used to capture interactions between chromatin and regulatory proteins, but it is unknown how stable most native interactions are. Although live-cell imaging suggests short-lived interactions at tandem gene arrays, current methods cannot measure rapid binding dynamics at single-copy genes. We show, by using a modified ChIP assay with subsecond temporal resolution, that the time dependence of formaldehyde cross-linking can be used to extract in vivo on and off rates for site-specific chromatin interactions varying over a ~100-fold dynamic range. By using the method, we show that a regulatory process can shift weakly bound TATA-binding protein to stable promoter interactions, thereby facilitating transcription complex formation. This assay provides an approach for systematic, quantitative analyses of chromatin binding dynamics in vivo.

The chromatin immunoprecipitation (ChIP) assay is an approach for determining where chromatin-binding factors interact with DNA sequences and as such has provided fundamental insight into where and how gene regulatory processes occur in cells. In the ChIP assay, cellular constituents are cross-linked with formaldehyde, the isolated chromatin is fragmented, and protein-DNA complexes are then recovered by immunoprecipitation using an antibody that detects a chromatin-associated protein of interest. DNA sequences in the immunoprecipitate are then inventoried by polymerase chain reaction. The assay accurately defines where proteins bind (*1*), but it provides limited information about how stable the interactions are. For example, a relatively high ChIP signal could reflect high-occupancy stable binding or that a low-occupancy dynamic interaction was trapped owing to the long formaldehyde incubation period used in standard assays. In fact, live-cell imaging approaches indicate that many chromatin interactions are exceedingly short-lived (*2*, *3*), although such techniques do not provide high-resolution data regarding chromatin binding location. Precise chromatin

[1]Department of Biochemistry and Molecular Genetics, University of Virginia Health System, Charlottesville, VA 22908, USA. [2]Center for Cancer Research Core Fluorescence Imaging Facility, Laboratory of Receptor Biology and Gene Expression, National Cancer Institute, National Institutes of Health, Bethesda, MD 20892, USA.

*These authors contributed equally to this work.
†Corresponding author. E-mail: auble@virginia.edu (D.T.A.); sb3de@virginia.edu (S.B.)

location information can be obtained by competition ChIP, a method that monitors the replacement rate by a differentially tagged factor of interest. However, the time resolution is limited to ~20 min owing to the delay required to generate the competitor species [e.g., (*4*–*6*)]. A general assay that provides quantitative measures of site-specific on and off rates is essential for defining chromatin regulatory events as they occur in vivo.

To measure chromatin-binding dynamics in vivo, we developed and applied a mathematical model based on standard principles of chemical kinetics that describes the dependence of ChIP signal on formaldehyde cross-linking time. In this method, which we call cross-linking kinetic (CLK) analysis (*7*), the mathematical relationship between cross-linking time and ChIP signal is used to extract the overall on rate (the product of the second order rate constant, k_a, and the chromatin binding factor concentration, C_{TF}), the off rate, k_d; and the fraction of bound chromatin sites at steady state, θ_b^0. If C_{TF} is known, then the value of k_a can be determined. From k_d, the half-life, $t_{1/2}$, of the chromatin complex can be calculated ($t_{1/2} = \ln 2/k_d$). Figure 1A illustrates the model for a chromatin interaction with a relatively high on rate (left) or low on rate (right). Both complexes have the same off rate, so the higher on rate gives rise to a higher fractional occupancy before addition of formaldehyde ($t = 0$). If formaldehyde cross-linking occurs rapidly as expected (supplementary text), then complexes will be cross-linked at this rapid rate driven by cross-linking kinetics (row labeled $t = 1$s), fixing the in vivo occupancy in each cell within the first few seconds. At longer formaldehyde incubation times, the unbound chromatin sites become occupied and cross-linked at a rate driven by k_aC_{TF}, resulting in an additional increase in the ChIP signal over time. Simulations (Fig. 1B) show this biphasic behavior. The inflection or "knee" in the curves reveals the fractional occupancy in the cell population within the first few seconds of cross-linking. To better constrain the model fits of the data, we made measurements with cells expressing two different concentrations of the transcription factor (TF) of interest and fit the two data sets simultaneously.

To test the CLK method, we analyzed Gal4 binding to the single upstream activation sequence in the *GAL3* promoter. The Gal4 system has provided a paradigm for transcriptional regulation (*8*), but the in vivo stability of the Gal4-promoter interaction has been the subject of debate (*9*, *10*). A quench-flow apparatus was adapted to acquire formaldehyde-treated samples on the subsecond time scale, and longer time points were obtained by hand mixing before quenching in glycine (supplementary text). As predicted by the simulations (Fig. 1 and figs. S2 and S3), the ChIP signal increased dramatically at short formaldehyde incubation times (<5 s) and then gradually after longer incubation times (Fig. 2A, blue curve). The time dependence of the ChIP signal substantiates several key aspects of the model (fig. S4), and other fundamental suppositions were validated experimentally. First, the steep increase in ChIP signal at short cross-linking times demonstrates that cross-linking occurred rapidly and that glycine efficiently quenched the reaction (Fig. 2, A and C), as stipulated in the model. The curve was shifted upward in cells with a 2.5-fold increase in Gal4 (Fig. 2A, red curve), consistent with the time dependence of the slower phase of the ChIP signal being driven by the overall on rate for Gal4 chromatin binding and not formaldehyde reaction kinetics. In the model, the ChIP assay rapidly captures specifically bound TFs but does not inactivate or nonspecifically cross-link the remaining TF pool. In fact, the Gal4-promoter interaction occurred in cells even when binding was induced after formaldehyde pretreatment (Fig. 2B). Thus, Gal4 was not nonspecifically inactivated by formaldehyde. Moreover, the levels of soluble Gal4 and other proteins were reduced less than twofold in cell extracts after formaldehyde incubation, and their apparent molecular weights were not detectably affected (Fig. 2D and fig. S1). In addition, ChIP signals were indistinguishable over an eightfold range of formaldehyde concentration (Fig. 2E), demonstrating that formaldehyde was not limiting in the reaction. CLK analysis revealed that the Gal4-*GAL3* interaction had a $t_{1/2}$ of about 10 min (Fig. 2A and table S9), suggesting that a single Gal4 complex facilitates multiple rounds of transcription initiation. Combined with the low fractional promoter occupancy (~0.17), we conclude that the *GAL3* gene is likely transcribed in infrequent bursts.

To better define the dynamic range of the CLK method, we analyzed two TFs whose widely divergent dynamic behavior could be independently measured by fluorescence recovery after photobleaching (FRAP). FRAP was possible in these cases because the fluorescently tagged factors interact with tandem arrays of binding sites, making the chromosomal loci visible by microscopy. The CLK measured $t_{1/2}$ for the interaction of Ace1–green fluorescent protein (GFP) with the *CUP1* gene array (*11*) was 11 s, in excellent agreement with the value of 31 s obtained by FRAP (Fig. 3, A and B, and table S8). The interaction of LacI-GFP with an array of *Lac* operators (*12*) was far more stable, and the two methods yielded $t_{1/2}$ values that differ by less than threefold (Fig. 3, C and D, and table S8). Thus, as validated by an independent approach, the CLK method can reveal rank-ordered estimates of TF-chromatin interaction stability over a wide range in vivo, including interactions that persist for mere seconds. Compared with other methods, the CLK method increases the time resolution of chromatin dynamics at single-copy loci by two to three orders of magnitude.

To further explore transcription dynamics using this method, we investigated the interaction of the TATA-binding protein (TBP) with each of seven different promoters possessing diverse transcriptional activities and driven by RNA polymerases (Pols) I, II, or III. Consistent with expectation (*13*), the Pol III–driven *SNR6* promoter had the highest occupancy; however, occupancies of all promoters were well below saturation (Fig. 4A and supplementary text). Moreover, TBP-promoter interactions varied dramatically, with $t_{1/2}$ values ranging from 1 to about 30 min (Fig. 4B and table S7), and in many cases half-lives were much shorter than distinguishable by any other technique. To test whether the method can quantify a dynamic difference associated with a perturbation in cellular transcription, we compared TBP dynamics in wild-type (WT) and *mot1-42* cells. Mot1 is an essential regulator of TBP, which uses its adenosine triphosphatase activity to dissociate TBP from DNA in vitro (*14*). Evidence supports a direct role for Mot1 in gene activation, but how it accomplishes this is unknown. By using *URA1* as a model Mot1-activated gene (*15*), we observed dramatically different CLK

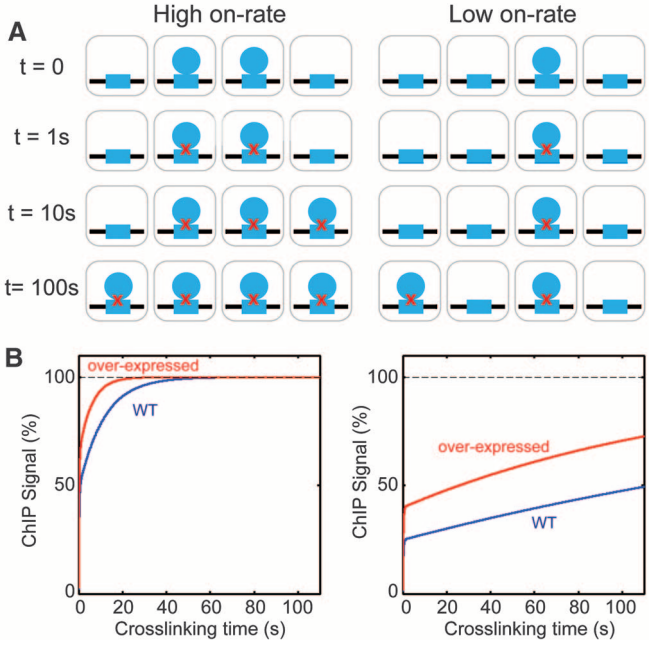

Fig. 1. Overview of the CLK model. (**A**) Schematic showing a chromatin site (blue rectangle) interacting with a transcription factor (blue circle) in a population of four cells in which chromatin binding has a relatively high (left) or low (right) on rate, but in both cases the off rate is the same. Rows descending from $t = 0$ show how the site occupancy in the cell population is predicted to change after addition of formaldehyde for 1, 10, or 100 s. Red X's indicate cross-linking. (**B**) Simulations of the two scenarios in (A) using the CLK model (blue lines). The red lines show simulations in which the TF concentration was increased threefold.

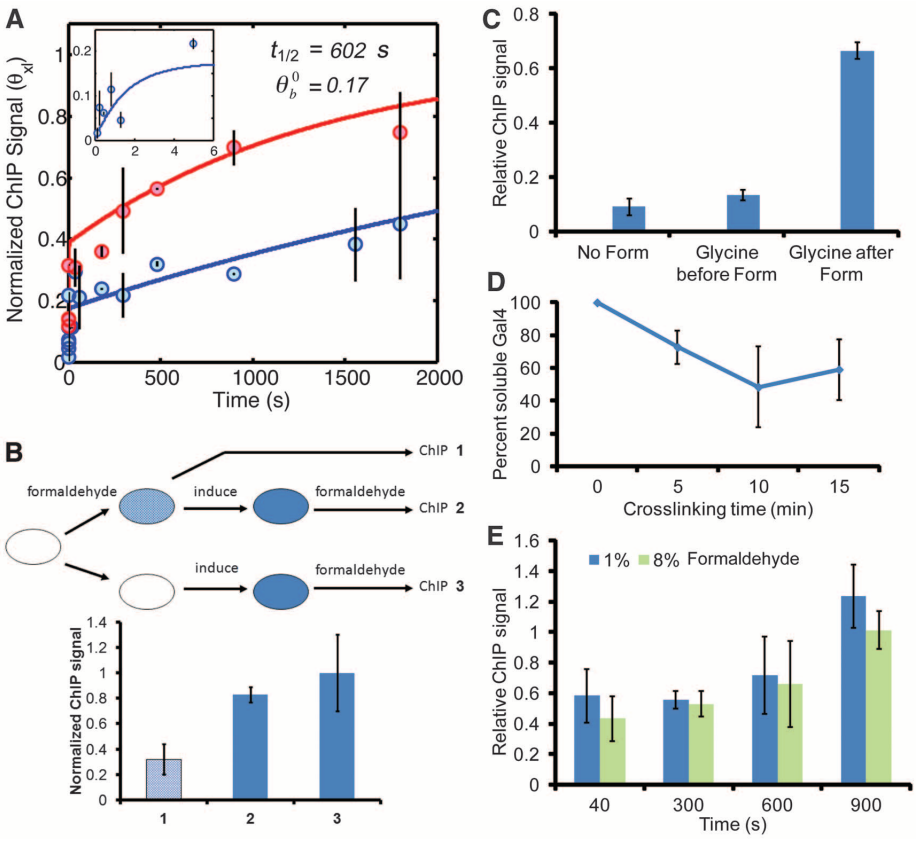

Fig. 2. CLK analysis of Gal4 and tests of model assumptions. (**A**) Model fits of CLK data for Gal4 binding to the *GAL3* promoter in cells with WT Gal4 levels (blue line) and cells with 2.5-fold overexpression of Gal4 (red line). (Inset) The first 5 s of a time course from cells with WT Gal4 levels. Error bars indicate SD. (**B**) Gal4 ChIP results obtained with cells treated as shown in the schematic. ChIP signals were obtained in formaldehyde-treated, uninduced cells (1), formaldehyde-treated cells subsequently induced by addition of galactose (2), and cells induced with galactose and subsequently treated with formaldehyde (3). Note that Gal4 chromatin binding was fully inducible in formaldehyde-treated cells. (**C**) Glycine addition before formaldehyde (Form) prevents crosslinking. The graph shows the relative Gal4 ChIP signal obtained when glycine was added before formaldehyde or 8 min after formaldehyde treatment, compared with cells in which no formaldehyde was added. (**D**) Relative soluble Gal4 protein level in extracts from cells treated with formaldehyde for the indicated times. Gal4 was quantified by Western blotting. (**E**) Gal4 ChIP signals at *GAL3* obtained by using cells treated with 1 or 8% formaldehyde for the indicated times. ChIP signals did not depend on formaldehyde concentration.

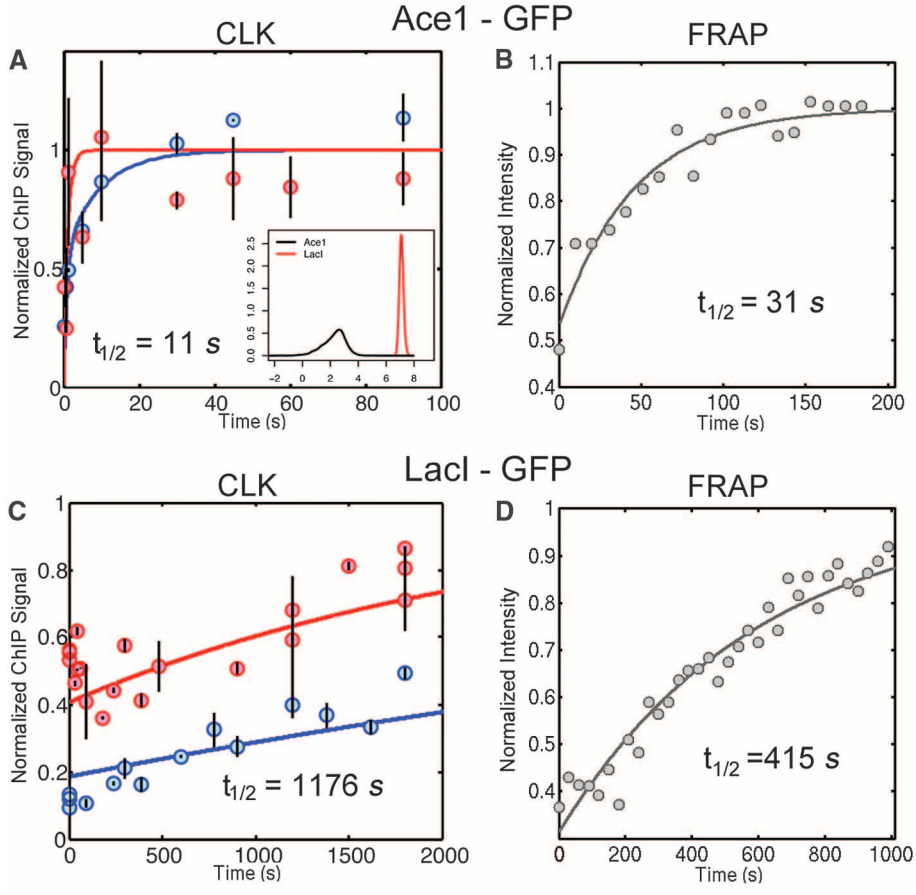

Fig. 3. Comparison of TF-chromatin dynamics by CLK and FRAP. (**A**) Model fits of CLK data for Ace1-GFP binding to *CUP1* in cells with two different expression levels of Ace1-GFP (low, blue curve; high, red curve; table S2). (Inset) Distributions of ln $t_{1/2}$ values obtained from multiple independent fits of the Ace1-GFP or LacI-GFP CLK data [shown in (C) and (*7*)]. (**B**) FRAP of Ace1-GFP in cells with low Ace1-GFP levels. (**C**) Model fits of CLK data for LacI-GFP binding to the *Lac* array in cells with low (blue curve) or high (red curve) levels of LacI-GFP (table S2). (**D**) FRAP of LacI-GFP in cells with low LacI-GFP levels.

curves for TBP binding to the *URA1* promoter in WT and *mot1-42* cells (Fig. 4C and table S7). Biochemical results suggested that Mot1 would activate *URA1* expression by displacing stably bound but inactive TBP from the promoter. However, mutation of Mot1 caused TBP binding to be far more dynamic than in WT cells (Fig. 4D). Similar results were observed at *INO1*, another Mot1-regulated promoter (fig. S13 and table S7).

To reconcile the CLK data with Mot1's biochemical activity and shed light on the process of transcription complex assembly in vivo, we compared the genome-wide TBP ChIP signal at a single cross-linking time in WT and *mot1-42* cells. Mutation of Mot1 increased the TBP ChIP signal at Pol II promoters, and the increase extended well outside the average nucleosome-free promoter region of about 200 base pairs and into flanking transcribed regions (Fig. 4E and fig. S14). TFIIB is a hallmark of transcriptional activity, but in contrast the TFIIB ChIP signal decreased over these same regions. Thus, unstable TBP complexes detectable in *mot1-42* cells were not associated with TFIIB and were transcriptionally inactive. Stable TBP complexes are apparently better substrates for TFIIB binding, and in turn the binding of TFIIB and other factors can block TBP clearance by Mot1 (*14*). Rather than catalyzing dissociation of stable interactions, these results reveal that Mot1 is responsible for dissociating weakly bound TBPs at diverse sites, thereby facilitating more stable TBP binding in functional transcription complexes. This enzyme-catalyzed change in TBP dynamics appears essential for proper gene expression; analogous processes may facilitate functional high-affinity chromatin binding at the expense of weak binding by other TFs as well.

The CLK assay yields estimates of physical kinetic parameters as opposed to relative rates, and it is applicable over a much broader time scale than competition ChIP because it is not limited by the time required to synthesize or activate a competitor molecule. This will permit rapid chromatin interaction dynamics for a factor to be compared directly to kinetic parameters for functionally related factors or processes. The CLK methodology is in principle not limited to yeast, and it is based on ChIP, one of the most widely used assays in chromatin research. Our data suggest an explanation for why there is no detectable stable chromatin-bound TBP as judged by live-cell imaging (*16*) but there are stable TBP complexes as judged by competition ChIP (*4*). The CLK results show that TBP fractional occupancies are low. Thus, although there are stable TBP-promoter complexes in vivo, most promoters are not occupied at steady state. The unexpectedly low occupancies are consistent with results showing that transcription in vivo occurs via uncoordinated stochastic cycles separated in time (*17*, *18*). CLK results also illustrate the danger of inferring relative occupancies or dynamics from ChIP assays using single, long formaldehyde incubation times. TBP ChIP signals are much greater in *mot1-42* cells than in WT cells, but the higher ChIP signals result from highly dynamic TBP molecules being trapped during the formaldehyde incubation period, rather than reflecting stable TBP binding.

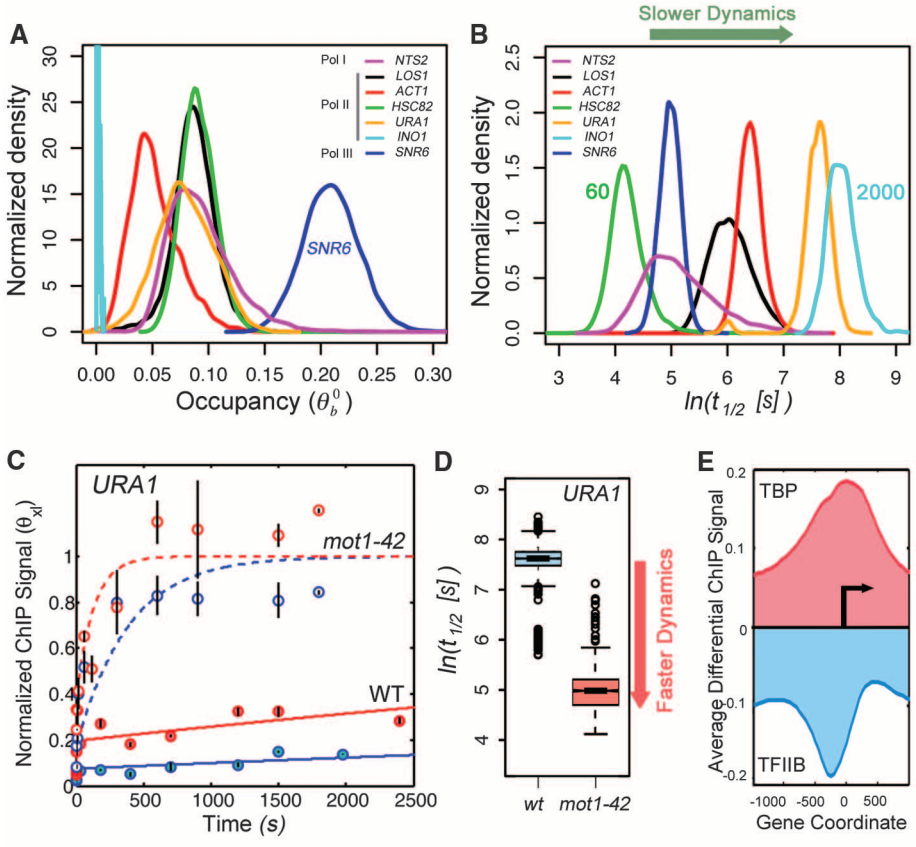

Fig. 4. TBP dynamics and regulation by Mot1. (**A**) Distributions of TBP occupancy at different yeast promoters obtained by multiple independent fits of the CLK data (*7*). (**B**) Distributions of TBP-promoter half-lives (*7*), whose mean values vary from 60 to about 2000 s. (**C**) Model fits of CLK data for TBP binding to the Mot1-activated *URA1* promoter in WT (solid lines) and *mot1-42* cells (dashed lines). Data and fits from cells expressing WT levels of TBP are shown in blue; results from cells overexpressing TBP are in red. (**D**) Box plots for distribution of $t_{1/2}$ values (log scale) for TBP binding to the Mot1-activated *URA1* promoter in WT (blue) and *mot1-42* cells (red). (**E**) Average genome-wide $\log_2$ differential TBP and TFIIB ChIP-chip signals at promoters in *mot1-42* versus WT cells shown with respect to the transcription start site (arrow) (*7*).

References and Notes

1. H. S. Rhee, B. F. Pugh, *Cell* **147**, 1408–1419 (2011).
2. G. L. Hager, J. G. McNally, T. Misteli, *Mol. Cell* **35**, 741–753 (2009).
3. M. E. van Royen, A. Zotter, S. M. Ibrahim, B. Geverts, A. B. Houtsmuller, *Chromosome Res.* **19**, 83–98 (2011).
4. F. J. van Werven, H. A. A. M. van Teeffelen, F. C. P. Holstege, H. T. M. Timmers, *Nat. Struct. Mol. Biol.* **16**, 1043–1048 (2009).
5. R. B. Deal, J. G. Henikoff, S. Henikoff, *Science* **328**, 1161–1164 (2010).
6. C. R. Lickwar, F. Mueller, S. E. Hanlon, J. G. McNally, J. D. Lieb, *Nature* **484**, 251–255 (2012).
7. Materials and methods are available as supplementary materials on *Science* Online.
8. A. Traven, B. Jelicic, M. Sopta, *EMBO Rep.* **7**, 496–499 (2006).
9. G. A. Collins, J. R. Lipford, R. J. Deshaies, W. P. Tansey, *Nature* **461**, E7 (2009).
10. K. Nalley, S. A. Johnston, T. Kodadek, *Nature* **461**, E8 (2009).
11. T. S. Karpova *et al.*, *Science* **319**, 466–469 (2008).
12. C. C. Robinett *et al.*, *J. Cell Biol.* **135**, 1685–1700 (1996).
13. D. N. Roberts, A. J. Stewart, J. T. Huff, B. R. Cairns, *Proc. Natl. Acad. Sci. U.S.A.* **100**, 14695–14700 (2003).
14. R. Viswanathan, D. T. Auble, *Biochim. Biophys. Acta* **1809**, 488–496 (2011).
15. R. O. Sprouse *et al.*, *J. Biol. Chem.* **283**, 24935–24948 (2008).
16. R. O. Sprouse *et al.*, *Proc. Natl. Acad. Sci. U.S.A.* **105**, 13304–13308 (2008).
17. D. R. Larson, D. Zenklusen, B. Wu, J. A. Chao, R. H. Singer, *Science* **332**, 475–478 (2011).
18. D. M. Suter *et al.*, *Science* **332**, 472–474 (2011); 10.1126/science.1198817.

Acknowledgments: We thank K. Struhl, F. Pugh, S. Hahn, and P. deHaseth for discussion; R. Nakamoto and M. Galkin for discussions and help with the KinTek instrument; and J. Muldoon, J. Hopper, F. Pugh, and S. Hahn for strains and plasmids. J.G.M. and T.S.K. were supported by the intramural program of the NIH, National Cancer Institute, Center for Cancer Research. Supported by NIH grant GM55763 to D.T.A.

Supplementary Materials

www.sciencemag.org/content/342/6156/369/suppl/DC1
Materials and Methods
Supplementary Text
Figs. S1 to S15
Tables S1 to S9
References (*19*–*37*)

25 June 2013; accepted 20 September 2013
Published online 3 October 2013;
10.1126/science.1242369